Articles

Solution Conformation of Cobrotoxin: A Nuclear Magnetic Resonance and Hybrid Distance Geometry–Dynamical Simulated Annealing Study†

Chin Yu,*,‡ R. Bhaskaran,‡,§ Li-Chin Chuang,‡ and Chen-Chung Yang‖

Chemistry Department and Institute of Life Science, National Tsing Hua University, Hsinchu, Taiwan, Republic of China

Received August 18, 1992; Revised Manuscript Received November 30, 1992

ABSTRACT: The solution conformation of cobrotoxin has been determined by using proton nuclear magnetic resonance spectroscopy. With the combination of various two-dimensional NMR techniques, the ^{1}H-NMR spectrum of cobrotoxin was completely assigned (Yu et al., 1990). A set of 435 approximate interproton distance restraints was derived from nuclear Overhauser enhancement (NOE) measurements. These NOE constraints, in addition to the 29 dihedral angle constraints (from coupling constant measurements) and 26 hydrogen bonding restraints (from the pattern of short-range NOEs), form the basis of 3-D structure determination by the hybrid distance geometry–dynamical simulated annealing method. The 23 structures that were obtained satisfy the experimental restraints, display small deviation from idealized covalent geometry, and possess good nonbonded contacts. Analysis of converged structures indicated that there are two antiparallel β sheets (double and triple stranded), duly confirming our earlier observations. These are well defined in terms of both atomic root mean square (RMS) differences and backbone torsional angles. The average backbone RMS deviation between the calculated structures and the mean structure, for the β-sheet regions, is 0.92 Å. The mean solution structure was compared with the X-ray crystal structure of erabutoxin b, the homologous protein. This yielded information that both structures resemble each other except at the exposed loop/surface regions, where the solution structure seems to possess more flexibility.

Cobrotoxin is a neurotoxic protein isolated in a crystalline state from the venom of Taiwan cobra (*Naja naja atra*) (Yang, 1965, 1967). It is a small, basic protein consisting of a single polypeptide chain of 62 amino acid residues, cross-linked by 4 disulfide bonds (Yang et al., 1969a,b). The complete amino acid sequence and the positions of disulfide bonds in cobrotoxin have been established (Yang et al., 1969a,b, 1970).

Cobrotoxin binds specifically to the nicotinic acetylcholine receptor on the postsynaptic membrane and thus blocks neuromuscular transmissions. Disulfide bonds and Tyr25, which are buried in the molecule, form a central core to maintain and stabilize the active conformation of the toxin (Chang et al., 1971a,b; Yang et al., 1974; Yang, 1987). Selective and stepwise chemical modifications of cobrotoxin indicate that at least two cationic groups, and the ϵ-amino group of Lys47 and a quanidino group of Arg33, both of which are common to all known postsynaptic snake neurotoxins, held at a certain critical distance in the molecule, are functionally important for its neuromuscular blocking activity (Chang et al., 1971a,b; Yang, 1974, 1988).

Recently, we reported ^{1}H-NMR resonance assignments to specific protons in cobrotoxin for over 95% of the backbone amide and Cα protons (Yu et al., 1990). These results were achieved by use of the sequential assignment technique, a two-dimensional NMR method developed by Wüthrich and co-workers (Anil Kumar et al., 1981; Wagner & Wüthrich, 1982; Rance et al., 1983; Wüthrich, 1986). The secondary structures of the antiparallel triple- and double-stranded β sheets were also determined by observing the NOEs for cobrotoxin (Yu et al., 1990). The investigation was further extended in order to determine the tertiary structure of cobrotoxin in aqueous solution, the results of which are reported here.

MATERIALS AND METHODS

Nuclear Magnetic Resonance Spectroscopy. Cobrotoxin was isolated and purified from the venom of Taiwan cobra (*Naja naja atra*) by chromatography on a SP-Sephadex C-25 column as described by Yang et al. (1981). It was further purified by reverse-phase HPLC on a column of TSK gel ODS-120T (preparative, 21.5 mm × 30 cm) obtained from Toyo Soda Manufacturing Co., Tokyo. Cobrotoxin samples were prepared in three different ways to attain various exchanged conditions for the amide protons of the protein. Nonexchanged cobrotoxin was prepared by dissolving lyophilized cobrotoxin (70 mg) in 90% H_2O/10% D_2O (0.5 mL, Merck) at 20 °C; this sample produces the spectrum of all amide protons. We prepared fully exchanged cobrotoxin by dissolving protein (70 mg) in D_2O and heating at 50 °C for 2 h; this sample produces the spectrum without labile amide protons. We prepared partially exchanged cobrotoxin by dissolving the protein in 99.95% D_2O at 5 °C; the spectrum of such a sample, measured at 5 °C, contains resonances from slowly exchanging amide protons.

All NMR spectra were recorded on a 400-MHz spectrometer (Bruker AM-400) equipped with an Aspect 3000 computer; 4,4-dimethyl-4-silapentane-1-sulfonate was used as an internal standard. NOESY (Jeener et al., 1979; Anil

† This work was supported by research grants from the National Science Council (NSC 81-0208-M-007-62 and NSC 81-0208-M-007-81) of the Republic of China.

* To whom correspondence should be addressed.

‡ Chemistry Department.

§ On leave from the Department of Physics, Bharathidasan University, Tiruchirapalli, India.

‖ Institute of Life Science.

0006-2960/93/0432-2131$04.00/0

Kumar et al., 1981; Macura et al., 1981) and DQF-COSY (Shaka & Freeman, 1983; Rance et al., 1983) spectra were recorded in D_2O with four different mixing periods, 50, 80, 130, and 300 ms for the NOESY experiments. Spectra taken in 90% H_2O/10% D_2O include DQF-COSY and NOESY experiments. Quadrature detection in ω_1 was achieved using time-proportional phase incrementation (Marion & Wüthrich, 1983). All homonuclear 2-D experiments (Ernst et al., 1987) were performed on a 20 mM protein sample; 768 t_1 increments were recorded, with 2048 complex points. For each free induction, the decays were Fourier-transformed on ω_2 using a Kaiser window and on ω_1 using a 45° phase-shifted sine-bell window. All two-dimensional data were processed on a μ-Vax computer (MV 3600) using the FTNMR software kindly provided by Dr. D. Hare.

Distance Restraints. About 95% of the assignments of the NH and Cα protons in the ^{1}H-NMR spectra of cobrotoxin have been reported earlier (Yu et al., 1990). During the course of this present study, the rest of the NH and Cα protons and a few additional assignments for side chain protons were made. Totally, a set of 435 interproton distance restraints were obtained from the analysis of NOESY spectra. The restraints are comprised of 192 intraresidue distances, 147 short-range [$(i - j) < 5$] interresidue distances, and 96 long-range [$(i - j) > 5$] interresidue distances. The NOEs were obtained by plotting the NOE build-up curves, for which the volumes of cross-peaks of the NOESY spectra were used for interpretation. The interproton distances, d_{ij}, were calculated according to the equation (Gondol & van Binst, 1986):

$$d_{ij} = d_{lm}(\sigma_{lm}/\sigma_{ij})^{1/6}$$

in which d_{lm} stands for a known calibrated distance (1.78 Å for geminal protons) and σ_{lm} and σ_{ij} stand for the cross-relaxation (NOE build-up) rate for spins l,m and i,j, respectively (obtained from the initial slope of the NOE build-up curve). The distance constraints involving the pseudoatoms were taken into consideration as described by Wüthrich et al. (1983).

Dihedral Angle Constraints. $^3J_{HN\alpha}$ coupling constants were obtained in the fingerprint region of the DQF-COSY spectrum using the peak to peak separation of the antiphase fine structure components in the contour plots. For $J_{HN\alpha}$ smaller than 5.5 Hz, ϕ was restricted to the range −90°,−40°; for $J_{HN\alpha}$ equal to 8.0 Hz, ϕ was restricted to −170°,−70°, and for large couplings with $J_{HN\alpha}$ greater than 10.0 Hz, the ϕ angle constraints were to the range −140°,−100°. Thus, the backbone dihedral ϕ angle restraints were obtained for 29 residues by using the Karplus (1963) relationship (Pardi et al., 1984).

Hydrogen Bonding Restraints. Backbone hydrogen bonds within the antiparallel β sheets were identified according to the criteria laid out by Wagner et al. (1987) which consists of the presence of NOEs between residues on opposite strands of an antiparallel β sheet in conjunction with slowly exchanging backbone amide protons; 13 slowly exchanging backbone NH protons [identified earlier by Yu et al. (1990)] could be easily assigned unambiguously in the above manner to hydrogen bonds within antiparallel β-sheet segments. These NH(i)–CO(j) hydrogen bonds are as follows: i,j = 5,13; 15,3; 13,5; 26,53; 28,51; 29,36; 27,38; 36,29; 38,27; 42,23; 52,28; 53,26; and 55,24 where i and j represent the residue positions of the two amino acids involved. In subsequent calculations, two restraints were used for each NH(i)–CO(j) backbone hydrogen bond with r(N–O) restricted to 2.4–3.3 Å and r(NH–O) to 1.7–2.3 Å.

Tertiary Structure Computations. Three-dimensional structures of cobrotoxin were computed by using the hybrid distance geometry–dynamical simulated annealing procedure of Nilges et al. (1988) employing the program X-PLOR (Brünger, 1992). A number of recent reprints have discussed the general methods of dynamical simulated annealing (Holak et al., 1988; Bycroft et al., 1991; Clore et al., 1991; Barlow et al., 1992; Li et al., 1992). Thus, only the details relevant to its present application will be presented here. In this approach, substructures which contain only about a third of the atoms were generated by projection from n-dimensional distance space using the metric matrix distance geometry algorithm. The rest of the atoms were fitted to the substructure, one residue at a time. These substructures were then used as the starting structures for the simulated annealing calculations. During the calculation, the S–S covalent bonds were deleted, and they were reintroduced as pseudo-NOE distances, with the S–S distances constrained to the upper limit of 2.1 Å. Thus, by this technique, the folding problem inherent in all real space methods is avoided, and the concept of simulated annealing is mainly used to effectively overcome potential energy barriers and search for the global minimum region by raising the temperature of the system initially followed by slow cooling.

A family of 40 substructures was generated using distance geometry (Brünger, 1992). After carrying out 200 cycles of Powell minimization on these substructures, a total of 10.19-ps dynamics were carried out following the procedure described by Brünger (1992) which is similar to that used in the hybrid distance geometry–simulated annealing protocol of Nilges et al. (1988) with some minor modifications. For these calculations, the energy function was assumed to contain only terms for bond lengths, bond angles, and improper torsions, a simple repulsion term, and a square-well potential to represent the NOEs and torsion angle restraints. No electrostatic, hydrogen bonding, or 6–12 Lennard–Jones van der Waals energy terms are used in the simulated annealing calculations (Nilges et al., 1988). During the first phase of the dynamics (2000 K), the values of the force constant of the NOE term were kept constant at 50 kcal/(mol·Å^2), and those of the repulsion and torsion angle terms were gradually increased from 0.03 to 4.0 kcal/(mol·Å^4) and from 5.0 to 200.0 kcal/(mol·rad^2), respectively. The resulting structures were finally subjected to 200 cycles of restrained (Powell) minimization with the full CHARMM energy function (Brooks et al., 1983).

Next, simulated annealing refinements were carried out on all these structures using the refinement protocol of Nilges et al. (Brünger, 1992) in order to remove the ill-behaved structures, based on the constraint satisfaction of each coordinate set in the family of generated structures. This is a slow-cooling protocol with an additional feature of "softening" of van der Waals repulsion to enable atoms to move through each other. This consists of an 8.84-ps cooling dynamics, followed by 200 cycles of Powell minimization. From the analysis of the resultant structures, 17 were discarded on the basis of an NOE energy cutoff value of 125.0 kcal/mol with no distance constraint violation greater than 0.5Å.

All computations were carried out on Silicon Graphics 4D/25 and 4D/35 work stations. The molecular graphics software QUANTA (version 3.2.3; Polygen/Moleculer Simulations Inc.) was used for the generation, display, analysis, and plotting of molecular structures.

RESULTS AND DISCUSSION

A total of 23 structures thus selected from the above procedure were superposed among them, and the superposition

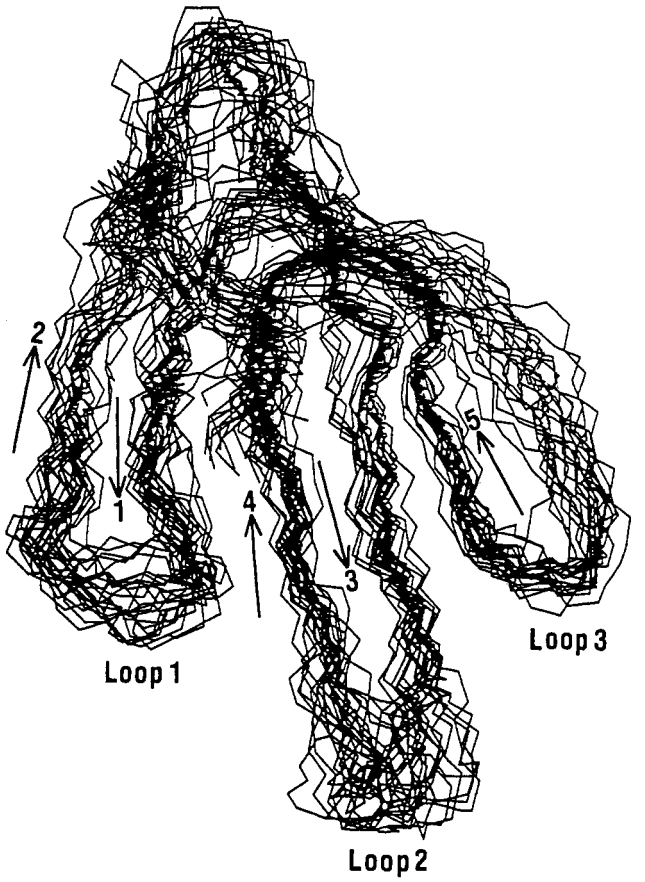

FIGURE 1: Superposition of the backbone (N, Cα, C′) atoms of the 23 solution structures of cobrotoxin. The three loops are indicated along with the strands (1–5) which are marked using arrows.

Table I: Structural Statistics[a]

	av of 23 structures
RMS deviations from idealized geometry used within X-PLOR	
bonds (Å)	0.0064
angles (deg)	0.8478
improper (deg)	0.6110
X-PLOR energy terms (kcal/mol)	
E_{NOE}	122.65
E_{cdih}	7.56
E_{L-J}	−252.60

[a] E_{L-J} is the Lennard–Jones van der Waals energy calculated with the CHARMM empirical energy function.

Table II: Average RMSD between the 23 Structures of Cobrotoxin and Respectively the Mean of These 23 Structures and the Crystal Structure of Erabutoxin b

		av RMSD (Å)	
ref structure	atoms considered	whole molecule	β-sheet segments
mean cobrotoxin structure	all	2.64	1.64
	backbone	1.67	0.92
crystal structure of erabutoxin b	backbone	2.65	2.17

of the backbone atoms (N, Cα, C′) of the structures is shown in Figure 1. The structures are well defined with proper tertiary folding. The structural statistics are presented in Table I; it is seen that the average RMS deviation from the mean structure is 1.67 Å for the backbone atoms and 2.64 Å for all atoms (Table II). The average atomic RMS deviation between the calculated structures and the mean structure versus residue number are shown in Figure 2.

It is clear from the structural statistics (Table I) that the calculated structures are in good agreement with the experimental data. The NOE connectivities and the short-range NEO pattern support the secondary structure identification. Thus, the nature of distance constraints indicates that only one family of structures exists rather than many differing structures. None of the structures have violations of the NOE constraints greater than 0.5 Å. The stereochemistry of the structures is good as judged by several criteria; all the φ angles (except the five residues found in the loop and turn) lie within the allowed regions of the Ramachandran plot (Ramachandran & Sasisekharan, 1968); the nonbonded contacts are characterized by a large negative Lennard–Jones van der Waals energy, and the deviations from the idealized covalent geometry are small (Table I). Thus, within this family, the structures are clearly very similar. The observation of low energy values reveals that the structures converged well to an acceptable stable conformation.

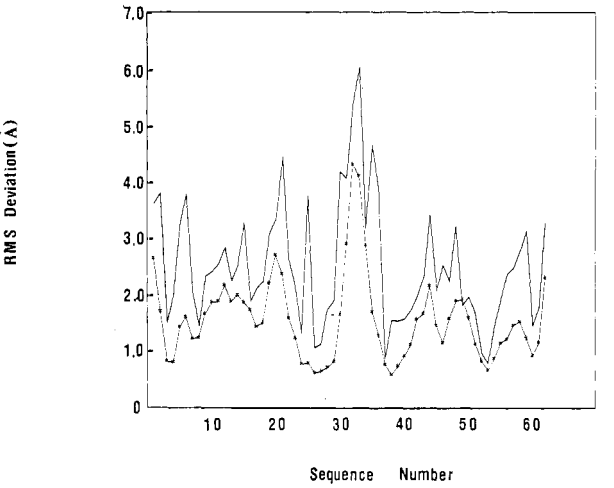

FIGURE 2: Distribution of the RMS difference of the 23 solution structures of cobrotoxin relative to the mean structure: backbone RMSD values were drawn by the thin line with an asterisk marking each residue position; side chain RMSD values were drawn by the thick line.

Description of the Structures. The secondary structural regions [as reported in our earlier article (Yu et al., 1990)] were identified both from the average backbone torsional angles and from the characteristic hydrogen bonding pattern. (The criteria used for hydrogen bonding is that the CO–NH distance is less than 3.3 Å and the N–H–O angle is greater than 130°.) Turns in the protein were identified when $i,i+3$ hydrogen bonds were present in all of the structures and were classified into types on the basis of characteristic coupling constants and the NOE pattern (Wüthrich, 1986).

From the selected structures, it is observed that three loops emerge from the globular head (as observed from the other short toxin family of structures). These three different loops contain five different strands to form two antiparallel β sheets, one double and one triple. Loop 1 (leftmost one) involves the two strands (strands 1 and 2) of the double-stranded β sheet. Loop 2 (middle loop) involves strands 3 and 4 of the triple-stranded β sheet; loop 3 (rightmost loop) contains strand 5. For both β sheets, their respective backbone dihedral angles are found to be in the allowed regions of the Ramachandran map for β sheets, duly confirming the observation of the secondary structures. The double-stranded antiparallel β sheet is found to be on the N-terminal side with the strand 1 range from Cys3 to Gln6 and the strand 2 range from Thr13 to Gly16. These two strands are linked by a three-turn (turn 1) segment (Gln7 to Glu10) which possesses a hydrogen bond between residues 7 and 10. This double-stranded β sheet is stabilized by hydrogen bonds between residues 3 and 15 and

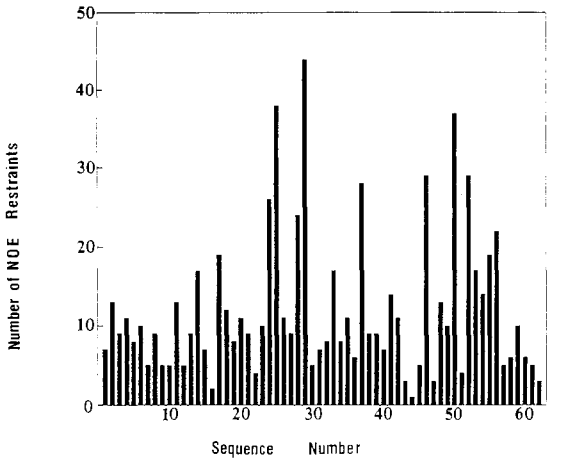

FIGURE 3: Schematic diagram showing the distribution of the NOE restraints used in the structure calculation.

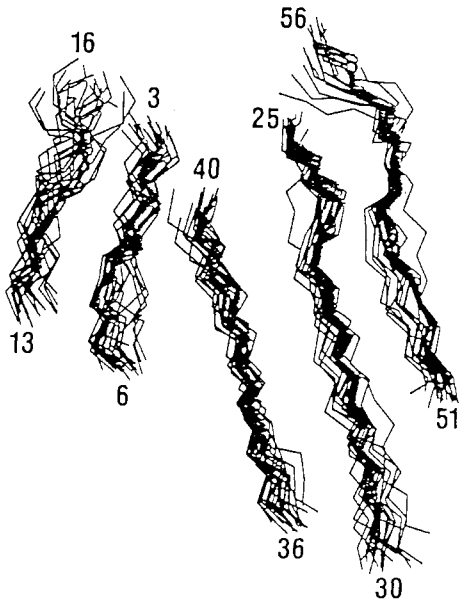

FIGURE 4: Superposition of the backbone (N, Cα, C′) atoms of the 23 solution structures of cobrotoxin showing both the double- and triple-stranded antiparallel β sheets.

between residues 5 and 13, each set forming two hydrogen bonds, respectively. This is connected to the triple-stranded β sheet by a larger segment containing residues 17–24. Since loop 1 is on the surface of the protein, projecting itself to the solvent (with a dominance of hydrophilic residues), it possesses higher flexibility in its conformations.

The triple-stranded antiparallel β sheet is formed among strand 3 (25–30), strand 4 (36–40), and strand 5 (51–56), in which strand 3 lies in between the two others. Strand 3 and strand 4 are connected by a three-turn (turn 2) segment; the residues involved are 31–34. Turn 2 is noted to have higher mobility because of its high exposure to solvent. Between the fourth and fifth strands, an eight-residue-long segment (42–49) is observed. This segment is found to have higher conformational freedom because the entire segment is exposed to solvent. This is confirmed by the highest peak noted in the RMSD plot for the mean structure (Figure 2), as also from the availability of lesser NOE constraints for these residues. This is observed from the plot for the distribution of the NOE restraints (Figure 3). The higher mobilities observed both for turn 2 and for the exposed segment in loop 3 may be due to the presence of cationic reactive groups (Arg33 and Lys47, respectively) which are expected to be functionally responsible

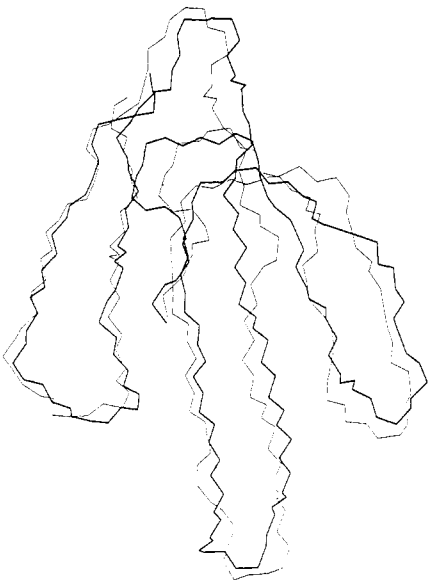

FIGURE 5: Superposition of the backbone (N, Cα, C′) atoms of the mean NMR structure (thin line) and the X-ray crystal structure of erabutoxin b (thick line).

for the neuromuscular blocking activity of the protein (Yang, 1988). The tail end possesses a folded conformation because of the disulfide bridge between residues Cys55 and Cys60.

In the superposition of the selected structures, barring the above-mentioned flexible regions, the overlap of the rest of the residues, in the β-sheet regions, is extremely good. Thus, the superposed plot of the backbone atoms of the 23 structures in their β-sheet regions is shown in Figure 4. They indicate a lower RMSD value (0.92 Å for the backbone atoms) than the mean structure (Table II).

Regarding the folding pattern, the backbone of the protein is folded in the following way: strand 4 runs antiparallel to strand 3 and folds in such a way to project itself outside, burying strand 3 in the interior. On the other hand, strand 5 runs antiparallel to strand 3 and makes the tail end direct outside to the opposite surface of strand 4. All the disulfide bonds are covalently linked such that they are all buried and converged at the globular head region by forming the central core of the molecule.

Comparison with the Crystal Structure of Erabutoxin b. The crystal structure of cobrotoxin has not yet been solved. Therefore, comparison of the NMR solution structure of cobrotoxin can only be made with the crystal structure of erabutoxin b, a homologous protein of the short toxin family, which has been solved to a resolution of 1.4 Å (Low & Corfield, 1986). A superposition of the backbone atoms of the mean solution structure and the X-ray structure of erabutoxin b is shown in Figure 5. A simple comparison of the structures shows that the secondary structure and overall fold are similar. The average RMS deviation between the structures is 2.65 Å for the backbone atoms. A comparison of the backbone torsional angles of the two structures indicates that only eight residues (Gly19, His32, Gly34, Gly42, Ser45, Val46, Asn48, and Gly49) have ϕ angles that deviate more than 60° between the structures. These residues are located within the exposed loop/turn regions, which are connecting the β strands of the protein. All the residues that have positive ϕ angles in the NMR solution structures also have positive ϕ angles in the X-ray crystal structure with the exception of residues His32, Val46, Lys47, and Asn48. Here again, the reason is because of their exposure to solvent.

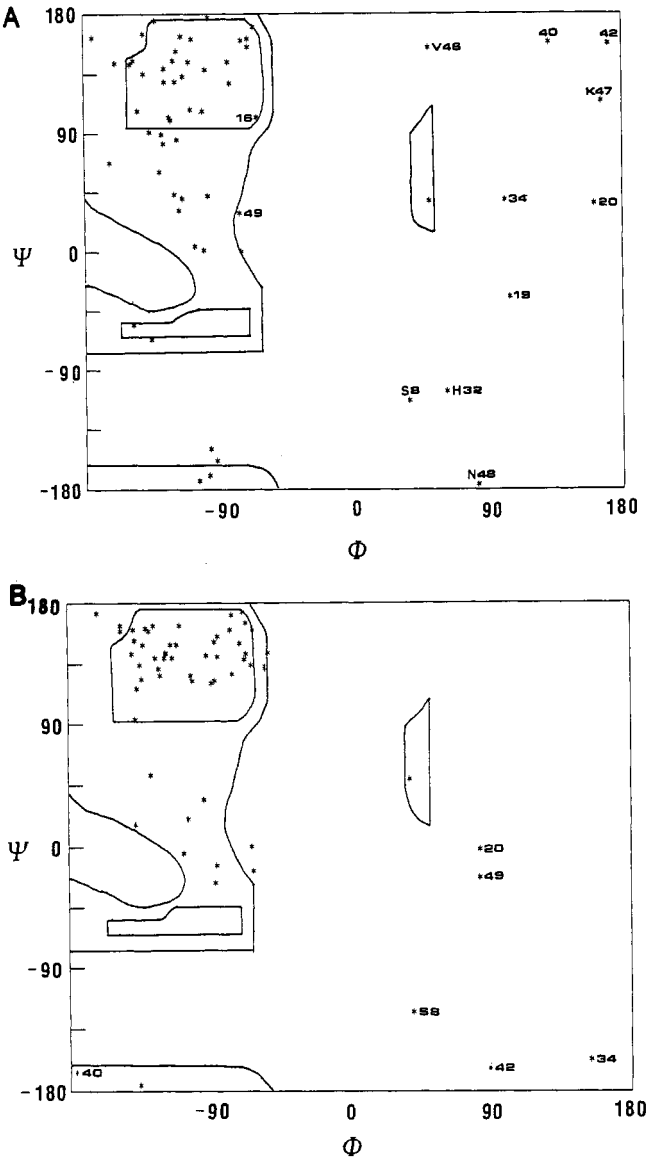

FIGURE 6: Ramachandran plots of the backbone conformational (ϕ, ψ) angles. (A) Plot for the mean NMR structure of cobrotoxin and (B) plot for the X-ray structure of erabutoxin b. The residue numbers of glycines are given and where the residues fall out of the allowed zones is indicated.

The agreement between the structures is best in the regions that contain regular secondary structures and worst in the exposed loops and turns. When the poorly defined regions of the NMR structure are excluded from the comparison, the average RMS deviation between the structures for residues 3–6, 13–16, 25–30, 36–41, and 51–56 is 2.17 Å for the backbone atoms. The regions where the largest deviations occur are also the least well defined in the NMR structure. It is probable that these variations exist because of the lack of definition of the NMR structure in these regions rather than any significant differences between the two structures.

The Ramachandran plots of the mean NMR solution structure of cobrotoxin and the crystal structure of erabutoxin b are shown in Figure 6 (panels A and B, respectively) for comparison. Figure 6B indicates that all the residues lie primarily in the energetically favorable regions of the Ramachandran map, with a clustering of points in the allowed region for the β sheet, confirming the presence of 50% β-sheet residues in the crystal structure. The observation of only one residue (Ser8) out of the favorable region reveals that the structure is stable without much mobility. Figure 6A (obtained

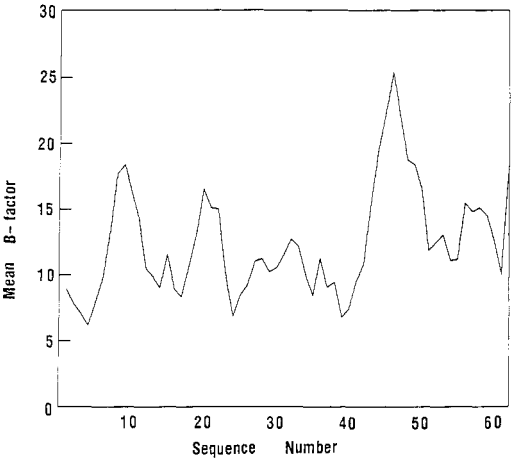

FIGURE 7: Variation of the mean *B*-factor values for crystalline erabutoxin b (Low & Corfield, 1986) for comparison with the distribution of the RMSD values from the mean NMR structure of cobrotoxin (Figure 2).

for the mean solution structure of cobrotoxin) also shows that most of the residues lie in the energetically favorable region. It is interesting that the two proline residues cluster around $\phi = -60°$. It is to be noted that no ϕ angle restraint was incorporated for proline residues during the course of the calculation. The residues that fall out of favorable zones in the ϕ,ψ plot, in addition to the glycine residues (with positive ϕ values), are Ser8 and His32 of the two turn regions and Val46, Lys47, and Asn48 of the exposed loop region. A comparison of the Ramachadran map of the two structures clearly reveals higher flexibilities for the residue range 42–49 in cobrotoxin compared to erabutoxin b.

In order to compare the mobilities of the residues, both in the mean solution structure of cobrotoxin and in the crystal structure of erabutoxin, the crystallographic thermal *B* factors of erabutoxin b (Low & Corfield, 1986) were compared with the RMSD values (Figure 2) of the mean NMR structure for backbone atoms. The variation in the *B* factors of erabutoxin b with its residue number is shown in Figure 7 for comparison with Figure 2.

A simple comparison of these figures indicates that both structures exhibit remarkable similar mobilities except at segments 7–10, 17–24, 31–35, 42–50, and 56–60, where higher mobilities are noted in the NMR structure of cobrotoxin. In the crystal structure, segment 42–50 is observed to have higher mobility than the rest of the structure. Similarly, as noted earlier, segment 31–35 seems to be extremely mobile with respect to the rest of the mean NMR structure. It is to be noted here that the same region was pointed out to be highly mobile in the NMR solution structure of α-cobratoxin (Goas et al., 1992). This region was identified as a short helix in α-cobratoxin. However, in cobrotoxin this was identified to be in a three-turn conformation. The antiparallel β-sheet residues (3–6, 13–16, 25–30, 36–41, and 51–56) are the most stabilized part in both structures. On the other hand, the loop 3 region, containing the reactive site residues, viz., Pro44, Arg46, Lys47, Gly49, and Ile50, is, in both cases, the mobile part of the protein, but the overall flexibility (backbone and side chain) is more in the solution structure compared to the crystal structure.

CONCLUDING REMARKS

In the solution structure of cobrotoxin, the antiparallel β-sheet regions are well defined, and in these regions, close agreement is noted between the NMR structure and the crystal structure of its homologous protein, erabutoxin b. The

conformation of the protein is, however, less well defined in turns and exposed loop segments. These ill-defined regions with greater mobility are expected to be the functionally important sites for accounting the receptor interactions.

ACKNOWLEDGMENT

We are grateful to Professor A. T. Brünger for providing X-PLOR software. The coordinates of 23 converged structures of cobrotoxin will be deposited in the Brookhaven Protein Data Bank.

REFERENCES

Anil Kumar, Wagner, G., Ernst, R. R., & Wüthrich, K. (1981) *J. Am. Chem. Soc. 103*, 3654–3658.

Barlow, P. N., Norman, D. G., Steinkasserer, A., Horne, T. J., Pearce, J., Driscoll, P. C., Sim, R. B., & Campbell, I. D. (1992) *Biochemistry 31*, 3626–3634.

Brooks, B. R., Bruccoleri, R. E., Olafson, B. D., States, D. J., Swaminathan, S., & Karplus, M. (1983) *J. Comput, Chem. 4*, 187–217.

Brünger, A. T. (1992) *X-PLOR Manual*, Yale University, New Haven, CT.

Bycroft, M., Ludvigsen, S., Fersht, A. R., & Poulsen, F. M. (1991) *Biochemistry 30*, 8697–8701.

Chang, C. C., Yang, C. C., Hamaguchi, K., Nakai, K., & Hayashi, K. (1971a) *Biochim. Biophys. Acta 236*, 164–173.

Chang, C. C., Yang, C. C., Nakai, K., & Hayashi, K. (1971b) *Biochim. Biophys. Acta 251*, 334–344.

Clore, G. M., Wingfield, P. T., & Gronenborn, A. M. (1991) *Biochemistry 30*, 2315–2323.

Ernst, R. R., Bodenhausen, G., & Wokaun, A. (1987) *Principles of Nuclear Magnetic Resonance in One and Two Dimensions*, Clarendon Press, New York.

Goas, R. L., LaPlante, S. R., Mikou, A., Delsuc, M. A., Guittet, E., Robin, M., Charpentier, I., & Lallemand, J. Y. (1992) *Biochemistry 31*, 4867–4875.

Gondol, D., & Van Binst (1986) *Biopolymers 25*, 977–983.

Holak, T. A., Nilges, M., Prestagard, J. H., Gronenborn, A. M., & Clore, G. M. (1988) *Eur. J. Biochem. 175*, 9–15.

Jeener, J., Meier, B. H., Bachmann, P., & Ernst, R. R. (1979) *J. Chem. Phys. 71*, 4546–4553.

Karplus, M. (1963) *J. Am. Chem. Soc. 85*, 2870–2871.

Li, X., Sutcliffe, M. J., Schwartz, T. W., & Dobson, C. M. (1992) *Biochemistry 31*, 1245–1253.

Low, B. W., & Corfield, P. W. R. (1986) *Eur. J. Biochem. 161*, 579–587.

Macura, C., Huang, Y., Suter, D., & Ernst, R. R. (1981) *J. Magn. Reson. 43*, 259–282.

Marion, D., & Wüthrich, K. (1983) *Biochem. Biophys. Res. Commun. 113*, 967–974.

Nilges, M., Gronenborn, A. M., & Clore, G. M. (1988) *FEBS Lett. 229*, 317–324.

Pardi, A., Billeter, M., & Wüthrich, K. (1984) *J. Mol. Biol. 180*, 741–751.

Ramachandran, G. N., & Sasisekharan, V. (1968) *Adv. Protein Chem. 23*, 283–437.

Rance, M., Sorensen, O. W., Bodenhausen, G., Wagner, G., Ernst, R. R., & Wurthrich, K. (1983) *Biochem. Biophys. Res. Commun. 117*, 479–485.

Shaka, A. J., & Freeman, R. (1983) *J. Magn. Reson. 51*, 169–173.

Wagner, G., & Wüthrich, K. (1982) *J. Mol. Biol. 155*, 347–366.

Wagner, G., Braun, W., Havel, T. F., & Wüthrich, K. (1987) *J. Mol. Biol. 182*, 295–315.

Wüthrich, K. (1986) *NMR of Proteins and Nucleic Acids*, Wiley, New York.

Wüthrich, K., Billeter, M., & Braun, W. (1983) *J. Mol. Biol. 169*, 949–961.

Yang, C. C. (1965) *J. Biol. Chem. 240*, 1616–1618.

Yang, C. C. (1967) *Biochim. Biophys. Acta 133*, 346–355.

Yang, C. C. (1974) *Toxicon 12*, 1–43.

Yang, C. C. (1987) in *Pharmacology* (Rand, M. J., & Raper, C., Eds.) pp 871–874, Elsevier Biomedical Division, Amsterdam.

Yang, C. C. (1988) *J. Chin. Biochem. Soc. 17*, 20–31.

Yang, C. C., Chang, C. C., Hayashi, K., & Suzuki, T. (1969a) *Toxicon 7*, 43–47.

Yang, C. C., Yang, H. J., & Huang, J. S. (1969b) *Biochim. Biophys. Acta 188*, 65–77.

Yang, C. C., Yang, H. J., & Chiu, R. H. C. (1970) *Biochim. Biophys. Acta 214*, 355–363.

Yang, C. C., Chang, C. C., & Liou, I. F. (1974) *Biochim. Biophys. Acta 365*, 1–14.

Yang, C. C., King, K., & Sun, T. P. (1981) *Toxicon 19*, 645–659.

Yu, C., Lee, C. S., Chuang, L. C., Shei, Y. R., & Wang, C. Y. (1990) *Eur. J. Biochem. 193*, 789–799.